

3D Radiative Hydrodynamic Modeling of the Near-Surface Shear Layer in the Solar Convection Zone

I. N. Kitiashvili¹, A. G. Kosovichev², A. A. Wray¹, V. M. Sadykov³, G. Guerrero^{2,4}

¹*NASA Ames Research Center, Moffett Field, Mountain View, CA 94035, USA*

²*New Jersey Institute of Technology, Newark, NJ 07102, USA*

³*Georgia State University, USA*

⁴*Universidade Federal de Minas Gerais, Brazil*

ABSTRACT

Understanding effects driven by rotation in the solar convection zone is essential for many problems related to solar activity, such as the formation of differential rotation, meridional circulation, and others. We present realistic 3D radiative hydrodynamics simulations of solar subsurface dynamics in the presence of rotation in a local domain 80 Mm-wide and 25 Mm deep, located at 30 degrees latitude. The simulation results reveal the development of a shallow 10-Mm deep near-surface shear layer (“leptocline”), characterized by a strong radial rotational gradient and self-organized meridional flows. This shear layer is located in the hydrogen ionization zone associated with enhanced anisotropic convective flows overshooting into a relatively stable zone between the H and HeII ionization zones. The radial variations of the differential rotation and meridional circulation profiles obtained from the simulations agree with helioseismic observations, indicating that a major role in forming the leptocline and subsurface meridional flows is played by the local Reynolds stresses.

Subject headings: The Sun, solar interior, solar convective zone, solar rotation, helioseismology, hydrodynamical simulations, radiative transfer simulations

1. Introduction

The discovery of solar rotation by Galileo Galilei and its variation with latitude by Christoph Scheiner through tracking sunspots across the disk was the first indication of complex processes associated with the Sun’s interior dynamics and activity. Intensive studies of

¹e-mail: irina.n.kitiashvili@nasa.gov

global dynamics using spectroscopic and sunspot observations and derivation of the properties of differential rotation stimulated theoretical investigations and data analysis developments. For a historical review of pre-helioseismology studies of the solar rotation, we will refer readers to the paper by Paternò (2010). The development of helioseismology techniques to probe solar internal structure and dynamics made it possible to investigate the properties and evolution of solar differential rotation and meridional circulation in the convection zone (e.g., Gough 1981; Kosovichev et al. 1997; Kosovichev 2006; Thompson et al. 1996, 2003; Howe 2009; Zhao et al. 2013; Basu & Antia 2019). Uninterrupted whole-disc observations of the Sun from space (SOHO and SDO) and the ground (e.g., SOLIS, GONG, Mt. Wilson Observatory) advanced the study of global solar dynamics from the deep interior to the surface (e.g., Deubner et al. 1979; Howard et al. 1983; Woodard 1989; Kosovichev et al. 1997; Birch & Kosovichev 1998; Schou et al. 1998; Howe et al. 2000; González Hernández et al. 2008; Ulrich 2010; Basu 2016; Antia & Basu 2022). Understanding physical processes associated with variations in differential rotation and meridional circulation can accelerate the development of new capabilities for modeling and predicting solar activity on various time scales.

Traditionally, the effects of solar rotation are modeled on global scales (e.g., Brun & Toomre 2002; Brun et al. 2011; Miesch & Hindman 2011; Guerrero et al. 2016, 2019; Stejko et al. 2020). However, global models face many challenges in reproducing the internal dynamics of the Sun correctly. Because of computational limitations, the global simulations are usually performed using an anelastic approximation that excludes the upper layers of the convection zone. To gain insight into the structure and dynamics of the upper layers of the convection zone in the presence of rotation, we perform local 3D radiative hydrodynamic modeling of the uppermost layers of solar convection. The computational model includes effects of compressibility, radiative energy transport, and subgrid-scale turbulence and reproduces solar convection with a high degree of realism. Currently, such simulations cannot be performed for the whole spherical Sun. Therefore, the computational domain is limited to a local region, in this case a rectangular volume 80 Mm wide and 25 Mm deep, located at 30 degrees latitude. The presentation of the results begins with a brief description of the numerical setup (Section 2). Then, Section 3 describes the thermodynamic and dynamical properties of convective and large-scale flows, particularly the self-formed subsurface shear layer and meridional flows. Finally, Section 4 discusses the main findings and compares them with observations.

2. Computational Setup

We perform 3D radiative hydrodynamic simulations using the StellarBox code (Wray et al. 2018). The formulation of the StellarBox code includes the fully compressible MHD equations from first principles plus radiative transfer. Rotational effects are modeled in the f -plane approximation. The computational model takes into account the realistic chemical composition and equation of state, and a large-eddy simulation (LES) treatment of sub-grid turbulent transport. The subgrid turbulence models (Smagorinsky 1963; Moin et al. 1991) are critical for accurately describing small-scale energy dissipation and transport. The radiative transfer calculations are performed for four spectral bins; ray-tracing along 18 directional rays (Feautrier 1964) is implemented using the long-characteristics method. The wavelength-dependent opacity code and data are provided by the Opacity Project (Seaton 1995; Badnell et al. 2005). The simulations are performed in Cartesian geometry. The lateral boundary conditions of the computational domain are periodic. The top boundary is open to the mass, momentum, energy fluxes, and radiation flux. The bottom boundary of the computational domain is open for radiation and simulates the energy input from the interior of the Sun. The simulations are initialized from a standard solar model of the interior structure and the lower atmosphere (Christensen-Dalsgaard et al. 1996).

This paper presents an analysis of a model with an imposed rotation corresponding to 30 degrees latitude. The extended duration of the simulations, over 200-hours, allows us to reach dynamically stationary conditions and investigate the influence of rotational effects. The horizontal size of the computational domain is 80 Mm \times 80 Mm, and the vertical domain extends to a depth of 25 Mm (Fig. 1). The grid resolution is 100 km in the horizontal directions; the vertical resolution varies from 50 km in the photosphere and low atmosphere to 82 km near the bottom boundary. The computational x-axis is oriented in the azimuthal direction, and the y-axis is directed toward the North pole. The bottom 5 Mm of the computational domain were excluded from the analysis to avoid potential boundary-related effects. The simulations include a 1 Mm high atmospheric layer. The data cubes are collected with a cadence of 45 sec.

3. Properties of the Solar Convection in the Near-Surface Shear Layer

Snapshots of the vertical velocity on the surface and in a radial slice of the computational domain are shown in Figure 1. Detailed properties of the granulation structure and dynamics are discussed in our previous papers (e.g., Kitiashvili et al. 2011, 2013a,b, 2015). In this paper, we focus on the effects of solar rotation.

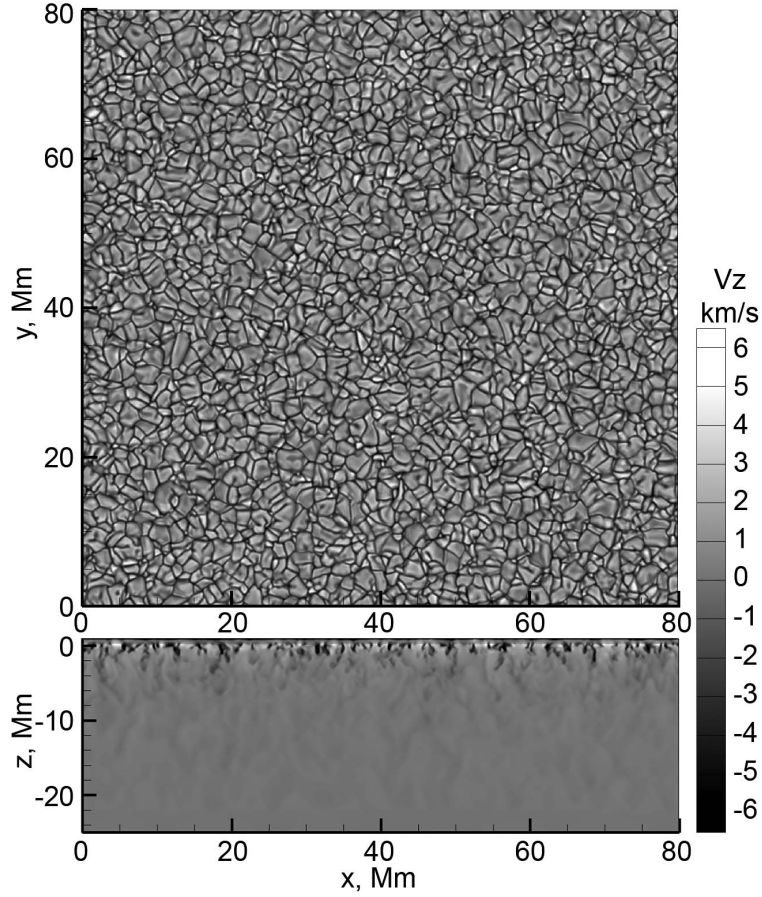


Fig. 1.— Snapshot of the vertical velocity at the solar photosphere (top panel) and a vertical slice through the computational domain (bottom).

To inspect deviations of the azimuthal flows from the imposed rotation, we calculate the radial profile of velocity along the direction of rotation (V_x) averaged in the horizontal directions and time. The results, shown in Figure 2a, reveal a significant decrease in the azimuthal velocity by 38 m/s in a 2 Mm deep layer below the photosphere. This means that the near-surface layers have lower rotation rate than the surface. Below 7 Mm, the rotation rate is slower than the imposed mean rotation rate by about 5 m/s. Interestingly, the rotation rate increase with the depth is not uniform: from the near-photosphere layers to about 4 Mm below, the velocity increases by 7–6 m/s per Mm, while below 4 Mm the flow accelerates by about 2 m/s per Mm. A similar change in the differential solar rotation rate at similar depths has been demonstrated in pioneering helioseismology observations by Deubner et al. (1979), where analysis of the $k - \omega$ diagram of solar oscillations showed a noticeable increase of the relative horizontal flows. The identified 10-Mm thick near-surface shear layer, or ‘leptocline’

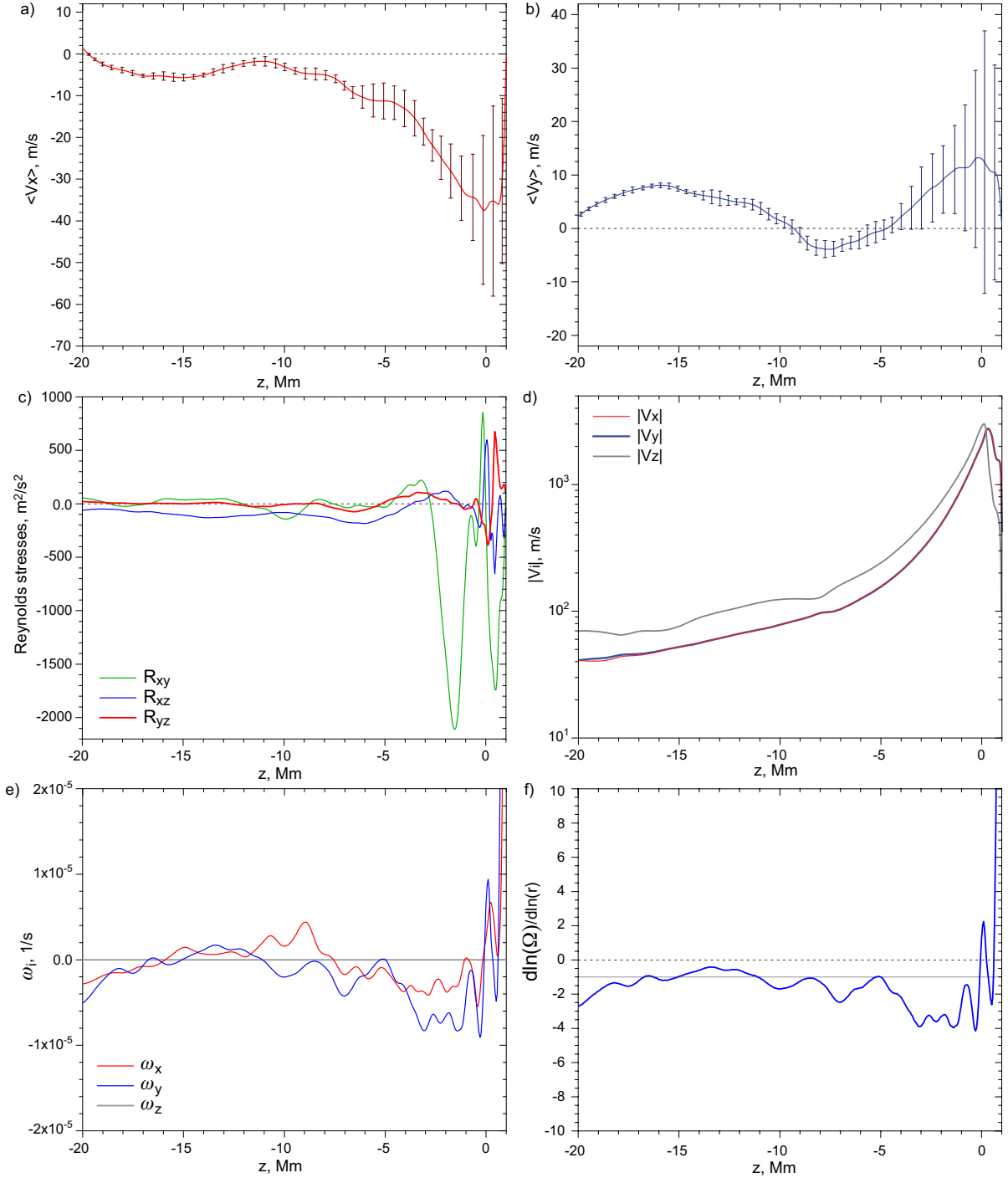


Fig. 2.— Mean radial profiles of a) deviations of the azimuthal flow speed from the imposed rotation rate at 30 degrees latitude, b) the meridional component of the flow velocity, c) profiles of the Reynolds stresses, d) the absolute values of the velocity components, e) the vorticity components, and f) the radial gradient of the local solar rotation rate, defined as $\frac{\partial \ln \Omega}{\partial \ln r}$. Radial profiles are obtained by averaging a 24-hour series of simulation data. Panels a) and b) show 1σ flow velocity deviations from the mean values.

(named by analogy from the tachocline and originated from greek *leptos* that means ‘fine’, Godier & Rozelot 1999, 2001), is clearly visible in the relative differential rotation profile (Figure 2a).

The meridional component of the mean velocity ($\langle V_y \rangle$, Figure 2b) reveals a complex structure with mostly poleward flows and a speed of $\sim 12 - 13$ m/s in the near-surface layers and about 8 m/s at a depth of 16 Mm. The meridional component of flow decelerates from the photosphere by 2.3 m/s per Mm to about -4 m/s at a depth of 8 Mm. Thus, a weak reverse flow occurs at 5 – 10 Mm depth. Below 8 Mm, the meridional flows accelerate again in the poleward direction.

The distribution of Reynolds stresses (computed as $R_{ij} = \overline{u'_i u'_j}$, where u'_i and u'_j are the velocity component fluctuations) reveals a complex coupling between the large-scale flows and small-scale turbulent motions (Figure 2c). It is not surprising that variations of the Reynolds stresses are strongest near the photosphere. In the absence of rotation or if rotation is too slow to influence the turbulence, it is expected that the mean horizontal component of the Reynolds stresses, R_{xy} , will have minimal variations. However, as shown in Figure 2c, the horizontal Reynolds stresses vary significantly from the low atmosphere down to layers about 4 Mm deep. In particular, strong variations of R_{xy} with a peak of -2111 m²/s² at a depth of 1.5 Mm correlate with the bottom of the granulation layer. The longitudinal (or azimuthal) component of the Reynolds stresses (R_{yz} , red curve) reveals strong variations near the photosphere. Below the photosphere, R_{yz} variations are weaker and vary around zero below 5 Mm. The meridional component of the Reynolds stresses is negative at the photosphere, revealing a sign change at the near-surface layers, where it reaches a maximum of ~ 100 m²/s² at a depth of 2 Mm. Below that, R_{xz} gradually decreases down to about 6 Mm below the surface and then fluctuates around -90 m²/s² in deeper layers of the convection zone.

In layers deeper than 5 Mm, there appears to be no preferred sign for horizontal Reynolds stresses, except in a 1 – 2 Mm thick layer at a depth of 10 Mm that indicates the presence of horizontal shear (green curve, Figure 2c). This layer corresponds to the bottom of the leptocline. This interface between the leptocline and deeper layers of the convection zone is manifested as a ‘bump’ in the horizontal flows and a ‘pit’ in vertical flows (Figure 2d), which signifies convective overshooting from the highly convectively unstable hydrogen ionization layers into a relatively stable layer between the H and HeII ionization zones.

In the presence of rotation, the radial profile of the mean vertical vorticity distribution (ω_z , Figure 2e, gray line) does not indicate preference of the vortical motions. On the other hand, the horizontal vorticity components (blue and red curves) reveal negative values, mostly in the top 5-Mm of the subsurface layers, which indicates a preference for clockwise

rotational turbulent flows. There is no significant directional preference for horizontal vorticity in the deeper layers, where the turbulence becomes more isotropic. Decrease of the horizontal vorticity around -18 - -20 Mm potentially due to closed bottom boundary for flow at depth -25 Mm and requires additional investigation for the deeper computational domain.

Helioseismic measurements show that the radial gradient of solar rotation, $\frac{\partial \ln \Omega}{\partial \ln r}$, (where Ω is the local angular velocity, r is solar radius) varies with latitude (Corbard & Thompson 2002), and has a value of about ~ -1 from the equator to 30 degrees latitude in the outer 15 Mm layer of the convection zone. At higher latitudes, the gradient is negative but has smaller values. These results have been confirmed by Barekat et al. (2014). More recent studies showed more substantial variations of the radial gradient with latitude. Also, the inferred radial profile depends on the selected range of spherical degree of solar oscillation modes used in the inversion procedure (e.g., ~ -2.8 for the high-degree inversions and -2.13 for the intermediate-degree inversion at 30 degrees latitude; Reiter et al. 2020). According to recent helioseismic studies by Antia & Basu (2022), the gradient changes with depth from ~ -0.95 at a depth of 7 Mm to -0.2 - -0.15 at a depth of 35 Mm.

Our results cover layers from the photosphere to 20 Mm below and show stronger negative values of the gradient of rotation, about -4 in subsurface layers, and an increase in the deeper layers (Figure 2f). Interestingly, the rotation gradient shows qualitatively the same variations as the meridional component of vorticity, ω_y , (blue curve, Figure 2e), which indicates coupling of the large-scale flows and turbulence. In the model, the gradient of rotation is shifted to lower values by about unity from the photospheric value obtained from high-spherical degree helioseismic inversions by Reiter et al. (2020), and values obtained by Antia & Basu (2022) for depths of 7 Mm and 20 Mm. The present discrepancies can be explained by the impact of solar activity on helioseismic inversions.

Because of the complexity of the mean flow distribution, it is interesting to consider how the velocity power spectra change with depth in the convection zone (Figure 3). As expected, the power is mainly concentrated in the near-surface flows and gradually decreases with depth. The rate of decrease reveals two sublayers (Figure 3a): 1) subsurface layers up to $7 - 8$ Mm, with a fast decrease, and 2) below 8 Mm, with a slow decrease. A spectral slope of $k^{-5/3}$ corresponds to a Kolmogorov-type inertial range at 1 Mm depth (Figure 3b). Similar changes with depth of the turbulent properties were previously demonstrated in simulations for a small (6.4 Mm wide and 5 Mm deep) computational domain (Kitiashvili et al. 2013b). A significant reduction in level of the velocity power distribution and the disappearance of the inertial range in the spectra for the deeper layers likely reflects a decrease of Reynolds number with depth. A weak increase of the kinetic energy at small wavenumbers,

$\sim 0.2 \text{ Mm}^{-1}$, indicates the presence of a convection scale of $\sim 20 \text{ Mm}$ that is comparable with the supergranulation scales. This scale becomes more prominent in the deeper layers. A more detailed study of this scale is required using a larger and deeper computational domain with a background magnetic field to determine its relation, if any, to observed supergranulation properties.

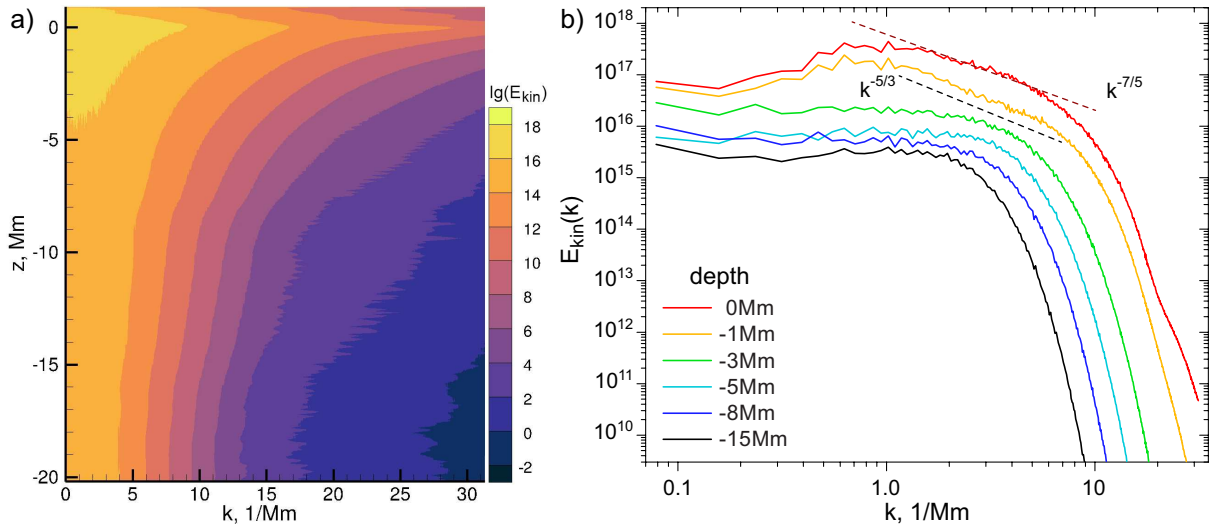


Fig. 3.— Averaged velocity power spectra. Panel a: Distribution with depth. Panel b: Spectra for several selected depths: from 15 Mm (black curve) to the photosphere (red).

In the presence of the rotation, it is natural to consider convection zone properties in terms of the Rossby number, the length scale of the turbulence, and the convective turnover time (Figure 4). Following Guerrero et al. (2019)’s suggestion, the length scale of the turbulent plasma is calculated as

$$\ell(r) = \frac{r \int_k \frac{\tilde{E}(k,r)}{k} dk}{\int_k \tilde{E}(k,r) dk},$$

where $\tilde{E}(k,r)$ is the velocity power spectral density, r is the solar radius, and k is the wavenumber. The convective turnover time is then $\tau_c = \ell(r)/V_{rms}$. The Rossby number can be expressed as $Ro = P_{rot}/(2\pi\tau_c)$, where P_{rot} is the rotational period.

According to our model, the Rossby number is the highest at the solar photosphere, where the turbulent flows are the strongest, and the convective turnover time is the shortest (Figure 4). It is known that the turbulent length-scale and the convective turnover time gradually increase with depth, resulting in a gradual decrease of the Rossby number in deeper layers. Interestingly, the length scale below the hydrogen ionization zone is almost

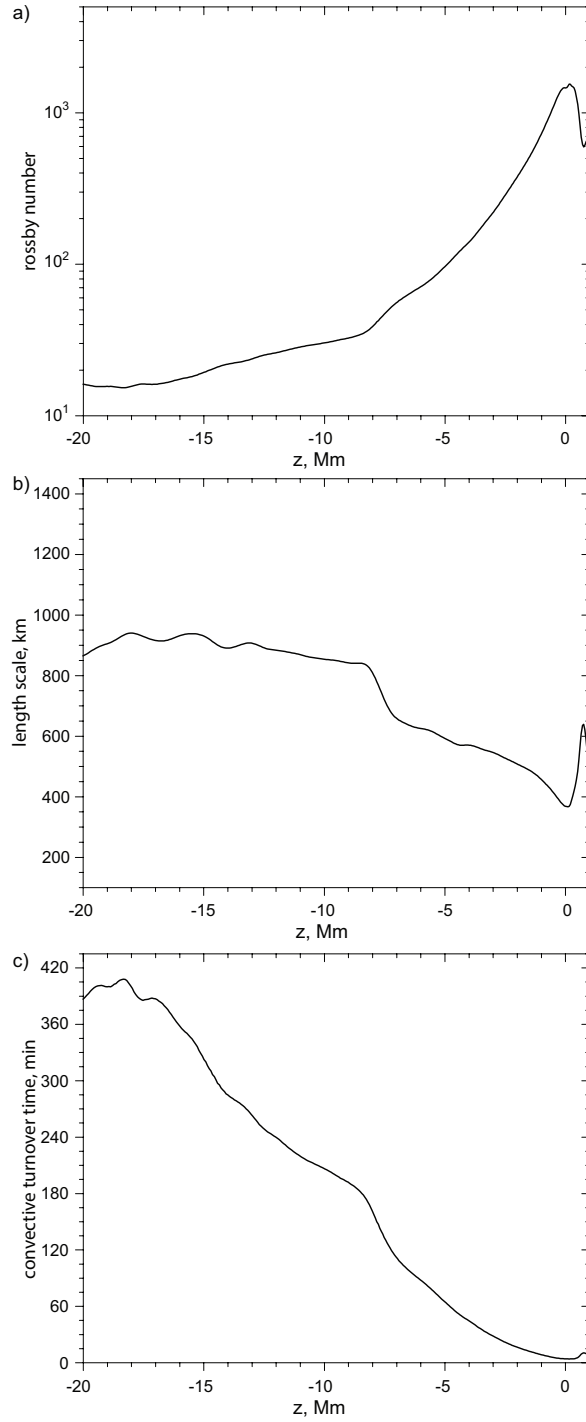


Fig. 4.— Radial profiles of the Rossby number (panel a), characteristic length scale (panel b), and convective turnover time (panel c). The profiles are time-averaged over 1 hour.

constant, with variations only around 100 km in the layers from 8 to 20 Mm below the solar surface (Figure 4b). However, the Rossby number decrease is not uniform. In particular, near the bottom of the hydrogen ionization zone, at a depth of 7 Mm below the surface, the length scale and the turnover time suddenly increase, thus slowing down the decrease of the Rossby number.

Because of plasma stratification, it is natural to consider how the temperature and density perturbations vary with radius (Figure 5a). In particular, the RMS temperature fluctuations (red curve) have a strong peak at the solar photosphere and exponentially decrease with depth. The radial profile becomes steeper at a depth of 8 Mm with a sudden reduction in temperature fluctuations. The thickness of the layer is about 1 Mm. The density fluctuations (blue curve) also reveal a sharp increase in the photosphere. In general, the RMS density fluctuations increase with depth up to 5 Mm below the photosphere and then become saturated. Similar to the temperature variations (red curve), the density variations sharply decrease in a 1 Mm-thick layer, near a depth of 8 Mm. This layer is located at the bottom of the hydrogen ionization zone (Figure 5b). The adiabatic exponent Γ_1 has a bump between 8 and 10 Mm, resulting in a layer of weaker convective instability between the hydrogen and second-helium ionization zones. This leads to convective overshooting effects, probably responsible for forming the shallow return meridional flow. Curiously, the shallow convective layer in the hydrogen ionization zone (the leptocline) seems to have some properties analogous to ones for the whole convection zone, such as convective overshooting, a tachocline, and return meridional flow.

4. Discussion and Conclusions

This paper discusses the effects of solar rotation on the dynamics and structure of the upper 20 Mm of the solar convection zone. Because of the weak influence of the relatively slow solar rotation on subsurface convection, we performed 3D radiative hydrodynamics simulations for 250 hours of solar time that allowed us to achieve steady dynamical conditions and provided a long dataset of more than 100 hours for analysis. We considered the dynamical and thermodynamic properties of solar convection from 20 Mm below the photosphere up to the lower atmosphere.

The simulation results reveal the development of radial differential rotation (Fig. 3a) with the strongest gradient in a 10 Mm-thick subsurface shear layer (a so-called leptocline). The existence of such a thin near-surface shear layer was previously suggested by Godier & Rozelot (1999, 2001). This boundary layer is characterized by an accelerated reduction of the Rossby number with depth and an increase in the length scale and convective

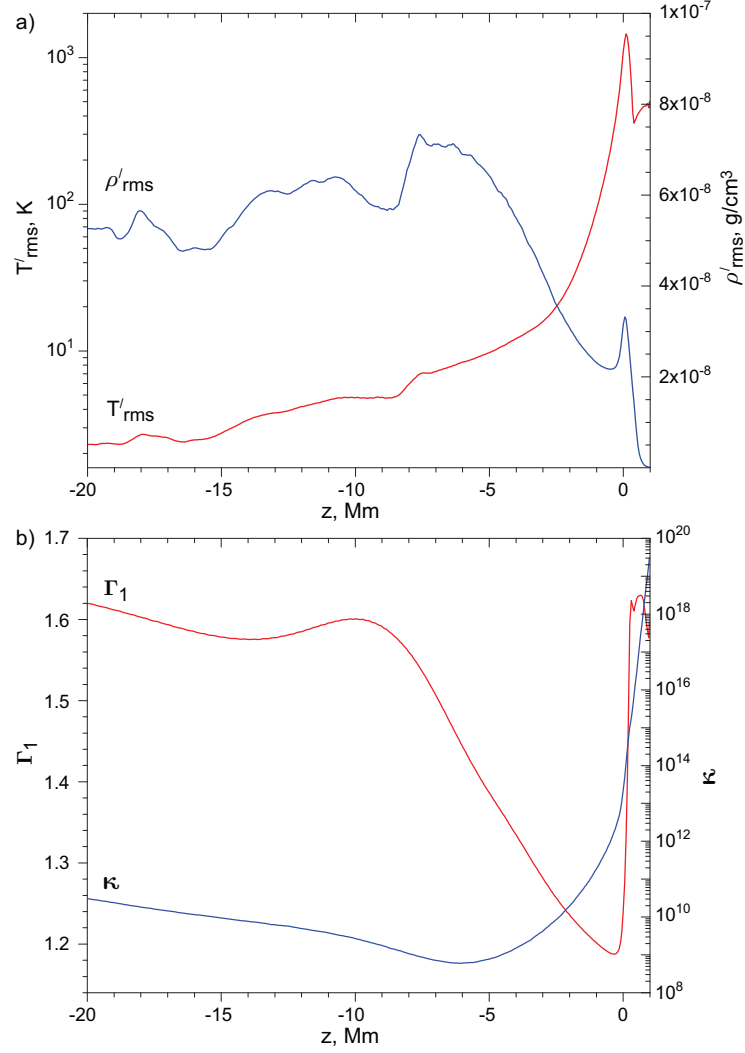


Fig. 5.— Panel a: Radial profiles of the temperature perturbations, T'_{rms} (red curve), and density perturbations, ρ'_{rms} (blue curve). Panel b: Radial profiles of the adiabatic index, Γ_1 (red curve) and the heat conductivity (blue curve). Radial profiles are time-averaged over 24 hours.

turnover time (Fig. 4). In terms of the thermodynamic properties, the bottom boundary of the leptocline is associated with a noticeable decrease of the temperature and density fluctuations (Fig. 5a) and is related to the bottom of the hydrogen ionization zone (Fig. 5b).

The resulting rotational velocity reduction relative to the imposed rotation rate of ~ 40 m/s at the photosphere is in agreement with observations near the solar minimum obtained with a variety of techniques (e.g. Hathaway & Rightmire 2010; Imada et al. 2020). It is important to note that the presence of a leptocline can be identified in multiple observations. The first indication of a 10-Mm thick subsurface layer was demonstrated by Deubner et al. (1979), using three one-day-long data series of observations, where inferences were made for every 2-Mm depth range up to 20 Mm below the photosphere. The recently developed new methods to perform more accurate rotational inversions allow distinguishing the leptocline in the radial rotational profiles (see Figure 27 in Reiter et al. 2020). According to these results, the leptocline is manifested as a steeper slope of the rotation rate near the photosphere, followed by a well-known subsurface shear layer with a weaker angular velocity gradient. Another helioseismic investigation, based on the ring-diagram analysis of SDO/HMI and GONG Dopplergrams, shows a qualitative change in the properties of the zonal flows at a depth of 8–10-Mm (see Figure 3 in Komm 2021), where the leptocline signature becomes more prominent for higher latitudes.

Another interesting feature of the leptocline is the presence of a convective overshoot at the bottom of the hydrogen ionization zone. It intensifies the mixing of the turbulent flows and explains why the velocity power spectrum changes below 10 Mm depth (Figure 3a). The overshoot layer (interface between the leptocline and deeper layers of the convection zone), was revealed from an analysis of the Reynolds stresses and variations of the velocity magnitude (Figures 2c and 4d) that indicate a splashing of the downflows. This interpretation is also supported by significant variations of the temperature and density fluctuations at the bottom of the hydrogen ionization zone (Figures 5).

In addition, our model with imposed rotation reveals the formation of meridional flow. At the photosphere, the flow is in the northward direction with a mean speed of 12 – 13 m/s. At a depth of 4 Mm, the flow changes direction to equatorward and reaches ~ -4 m/s at a depth of 8 Mm. The reverse meridional flows correspond to the interface between the near-surface shear layer discussed above (leptocline) and the rest of the convection zone. In the deeper layers, the flows accelerate again and change direction to northward at a depth of 10 Mm. At a depth of 16 Mm, the mean velocity reaches the speed of 8 m/s. The described near-surface flows suggest a possibility of fine structuring, similar to previously discovered two-cell meridional circulation on the scale of the whole convection zone (Zhao et al. 2013).

It is known that the properties of the meridional flows vary during the solar cycle. For

comparison with observations, we consider only observational studies that occur at a minimum of solar activity (or close to it) at 30 degrees latitude as the most relevant conditions to the hydrodynamic simulations. In general, we found a good agreement of the resulting meridional flows with surface (e.g., Ulrich 2010; Hathaway & Rightmire 2010; Hathaway & Upton 2014; Imada & Fujiyama 2018) and subsurface helioseismic inferences (e.g., Zhao et al. 2012; Komm et al. 2018; Antia & Basu 2022). The previous helioseismic studies reveal a qualitatively similar distribution of the meridional flows (e.g. Kosovichev & Zhao 2016; Komm et al. 2018): deceleration from the photosphere to 8–10 Mm and its acceleration at the deeper layers. In particular, Figure 8b in Kosovichev & Zhao (2016) shows that the meridional flows are getting weaker at a depth of 6 – 11.5 Mm and become stronger again with values comparable with the near-surface speed at a depth of 19 Mm. Perhaps the resolution of the helioseismic inversions was not sufficient to resolve the shallow layer with the return flow, and it was observed as a reduction in the flow speed. Indeed, more precise helioseismic measurements of the leptocline are needed.

To summarize the presented analysis of the 3D radiative hydrodynamics simulations with imposed rotation corresponding to 30 degrees latitude, we can identify the following main results:

- The simulations reveal the development of radial differential rotation and formation of a ~ 10 Mm-thick near-surface shear layer (leptocline), associated with a steep radial gradient of the angular velocity, changes in the thermodynamic and structural properties of the convection, and the bottom of the hydrogen ionization zone.
- The interface between the leptocline and the rest of the convection zone is characterized by a weak overshoot layer that may intensify the turbulent mixing in the layer.
- The self-formed meridional flows are characterized by poleward mean motions near the photosphere and weak reverse flows at depths of 5 – 10 Mm. The bottom of the reverse flows corresponds to the bottom of the leptocline layer and the hydrogen ionization zone. This structure resembles a double-cell meridional circulation previously found on the whole-convection-zone scale.
- The discussed agreement of the presented results with previous observational surface and subsurface properties of the differential rotation and meridional circulation demonstrates an ability to capture the physics of large-scale solar dynamics by performing 3D ‘ab-initio’ radiative hydrodynamic modeling on local scales.

The next step of this work is to perform modeling for different latitudes and investigate the latitudinal structure and dynamics of the leptocline.

Acknowledgments

The modeling and data analysis of the resulting data are performed using the NASA Ames Supercomputing Facility. The presented investigation is supported by NASA Heliophysics Supporting Research Program grant: NNX14AB70G, and NASA DRIVE Science Centers grant: 80NSSC20K0602 (COFFIES).

REFERENCES

- Antia, H. M., & Basu, S. 2022, *ApJ*, 924, 19
- Badnell, N. R., Bautista, M. A., Butler, K., et al. 2005, *MNRAS*, 360, 458
- Barekat, A., Schou, J., & Gizon, L. 2014, *A&A*, 570, L12
- Basu, S. 2016, *Living Reviews in Solar Physics*, 13, 2
- Basu, S., & Antia, H. M. 2019, *ApJ*, 883, 93
- Birch, A. C., & Kosovichev, A. G. 1998, *ApJ*, 503, L187
- Brun, A. S., Miesch, M. S., & Toomre, J. 2011, *ApJ*, 742, 79
- Brun, A. S., & Toomre, J. 2002, *ApJ*, 570, 865
- Christensen-Dalsgaard, J., Dappen, W., Ajukov, S. V., et al. 1996, *Science*, 272, 1286
- Corbard, T., & Thompson, M. J. 2002, *Sol. Phys.*, 205, 211
- Deubner, F. L., Ulrich, R. K., & Rhodes, E. J., J. 1979, *A&A*, 72, 177
- Feautrier, P. 1964, *Comptes Rendus Academie des Sciences (serie non speciffee)*, 258, 3189
- Godier, S., & Rozelot, J. P. 1999, in *ESA Special Publication, Vol. 9, Magnetic Fields and Solar Processes*, ed. A. Wilson & et al., 111–115
- Godier, S., & Rozelot, J. P. 2001, *Sol. Phys.*, 199, 217
- González Hernández, I., Kholikov, S., Hill, F., Howe, R., & Komm, R. 2008, *Sol. Phys.*, 252, 235
- Gough, D. O. 1981, *MNRAS*, 196, 731

- Guerrero, G., Smolarkiewicz, P. K., de Gouveia Dal Pino, E. M., Kosovichev, A. G., & Mansour, N. N. 2016, *ApJ*, 828, L3
- Guerrero, G., Zaire, B., Smolarkiewicz, P. K., et al. 2019, *ApJ*, 880, 6
- Hathaway, D. H., & Rightmire, L. 2010, *Science*, 327, 1350
- Hathaway, D. H., & Upton, L. 2014, *Journal of Geophysical Research (Space Physics)*, 119, 3316
- Howard, R., Adkins, J. M., Boyden, J. E., et al. 1983, *Sol. Phys.*, 83, 321
- Howe, R. 2009, *Living Reviews in Solar Physics*, 6, 1
- Howe, R., Komm, R., & Hill, F. 2000, *Sol. Phys.*, 192, 427
- Imada, S., & Fujiyama, M. 2018, *ApJ*, 864, L5
- Imada, S., Matoba, K., Fujiyama, M., & Iijima, H. 2020, *Earth, Planets, and Space*, 72, 182
- Kitiashvili, I. N., Abramenko, V. I., Goode, P. R., et al. 2013a, *Physica Scripta Volume T*, 155, 014025
- . 2013b, *Physica Scripta Volume T*, 155, 014025
- Kitiashvili, I. N., Couvidat, S., & Lagg, A. 2015, *ApJ*, 808, 59
- Kitiashvili, I. N., Kosovichev, A. G., Mansour, N. N., & Wray, A. A. 2011, *ApJ*, 727, L50
- Komm, R. 2021, *Sol. Phys.*, 296, 174
- Komm, R., Howe, R., & Hill, F. 2018, *Sol. Phys.*, 293, 145
- Kosovichev, A. G. 2006, *Advances in Space Research*, 37, 1455
- Kosovichev, A. G., & Zhao, J. 2016, *Reconstruction of Solar Subsurfaces by Local Helioseismology*, ed. J.-P. Rozelot & C. Neiner, Vol. 914, 25
- Kosovichev, A. G., Schou, J., Scherrer, P. H., et al. 1997, *Sol. Phys.*, 170, 43
- Miesch, M. S., & Hindman, B. W. 2011, *ApJ*, 743, 79
- Moin, P., Squires, K., Cabot, W., & Lee, S. 1991, *Physics of Fluids A*, 3, 2746
- Paternò, L. 2010, *Ap&SS*, 328, 269

- Reiter, J., Rhodes, E. J., J., Kosovichev, A. G., et al. 2020, *ApJ*, 894, 80
- Schou, J., Antia, H. M., Basu, S., et al. 1998, *ApJ*, 505, 390
- Seaton, M. J. 1995, *The opacity project*
- Smagorinsky, J. 1963, *Monthly Weather Review*, 91, 99
- Stejko, A. M., Guerrero, G., Kosovichev, A. G., & Smolarkiewicz, P. K. 2020, *ApJ*, 888, 16
- Thompson, M. J., Christensen-Dalsgaard, J., Miesch, M. S., & Toomre, J. 2003, *ARA&A*, 41, 599
- Thompson, M. J., Toomre, J., Anderson, E. R., et al. 1996, *Science*, 272, 1300
- Ulrich, R. K. 2010, *ApJ*, 725, 658
- Woodard, M. F. 1989, *ApJ*, 347, 1176
- Wray, A. A., Bensassiy, K., Kitiashvili, I. N., Mansour, N. N., & Kosovichev, A. G. 2018, *Realistic Simulations of Stellar Radiative MHD*, ed. J. P. Rozelot & E. S. Babayev, 39
- Zhao, J., Bogart, R. S., Kosovichev, A. G., Duvall, Jr., T. L., & Hartlep, T. 2013, *ApJ*, 774, L29
- Zhao, J., Nagashima, K., Bogart, R. S., Kosovichev, A. G., & Duvall, T. L., J. 2012, *ApJ*, 749, L5